Astronomy & Astrophysics manuscript no. hot-loop-2d_JK_ver3a
December 1, 2014
©ESO 2014

New analytical and numerical models of a solar coronal loop: I. Application to forced vertical kink oscillations

K. Murawski[1], A. Solov'ev[2], J. Kraśkiewicz[1], and A.K. Srivastava[3]

[1] Group of Astrophysics, University of Maria Curie-Skłodowska, ul. Radziszewskiego 10, 20-031 Lublin, Poland
[2] Central (Pulkovo) Astronomical Observatory, Russian Academy of Sciences, St. Petersburg, Russia
[3] Department of Physics, Indian Institute of Technology (Banaras Hindu University), Varanasi-221005, India

December 1, 2014

arXiv:1411.7465v1 [astro-ph.SR] 27 Nov 2014

ABSTRACT

Aims. We construct a new analytical model of a solar coronal loop that is embedded in a gravitationally stratified and magnetically confined atmosphere. On the basis of this analytical model, we devise a numerical model of solar coronal loops. We adopt it to perform the numerical simulations of its vertical kink oscillations excited by an external driver.
Methods. Our model of the solar atmosphere is constructed by adopting a realistic temperature distribution and specifying the curved magnetic field lines that constitute a coronal loop. This loop is described by 2D, ideal magnetohydrodynamic equations that are numerically solved by the FLASH code.
Results. The vertical kink oscillations are excited by a periodic driver in the vertical component of velocity, acting at the top of the photosphere. For this forced driver with its amplitude 3 km s^{-1}, the excited oscillations exhibit about 1.2 km s^{-1} amplitude in their velocity and the loop apex oscillates with its amplitude in displacement of about 100 km.
Conclusions. The newly devised analytical model of the coronal loops is utilized for the numerical simulations of the vertical kink oscillations, which match well with the recent observations of decay-less kink oscillations excited in solar loops. The model will have further implications on the study of waves and plasma dynamics in coronal loops, revealing physics of energy and mass transport mechanisms in the localized solar atmosphere.

Key words. MHD - Magnetic fields - Corona - Waves

1. Introduction

The solar corona is a magnetically dominated and gravitationally stratified medium which can alter the scenario of magnetohydrodynamic (MHD) waves (e.g., Pascoe 2014). Among a number of magnetic structures present there, the magnetic loops are considered as a major building blocks of the solar corona. They are outlined by curved and closed magnetic field lines, which are rooted in the deep atmospheric layers, and are built of the denser and hot plasma.

Coronal loops act as a waveguide for various kinds of magnetohydrodynamic (MHD) waves and oscillations. Among various modes, the standing, large-amplitude magnetoacoustic kink waves in coronal loops were detected in the solar coronal loops (e.g., Aschwanden et al. 1999, Aschwanden et al. 2000, Wang & Solanki 2004, Wang et al. 2008, Verwichte et al. 2009, Aschwanden & Schrijver 2011, White et al. 2012, Srivastava & Goossens 2013, and references therein). These transverse (horizontally and vertically polarized) kink waves are modeled by a number of authors (e.g., Gruszecki et al. 2006, Ofman & Wang 2008, Ofman 2009, Luna et al. 2010, Selwa et al. 2011, Antolin et al. 2014, and references therein) who confirmed the observational data by revealing that these waves decay on a time-scale comparable to the oscillation wave-period. Recently, small amplitude transverse waves were reported by De Moortel & Nakariakov (2012), Nisticó et al. (2013) and Anfinogentov et al. (2013) who found decay-less oscillations with velocity amplitude of few km s^{-1}, the displacement amplitude less than 1 Mm, and wave-periods within the range of 2.5 to 11 min.

The wave and plasma dynamics of coronal loops highly depend upon their plasma and magnetic field structuring. The analytical models of coronal loops were devised so far for a gravity-free medium and the loop oscillations were triggered by impulsive sources in most of the theoretical studies. Our aim here is to construct for the first time an analytical model of a coronal loop in a gravitationally stratified solar atmosphere. As the problem is formidable, we limit ourselves to the simplest conceivable case of a two-dimensional (2D) model of a coronal arcade loop. As a result of very long (few thousand lines) analytical expressions which result in the analytical model for the equilibrium mass density and a gas pressure, we focus ourselves on the modest case of a loop. On the basis of our analytical model, we develop a numerical model of a loop. The newly developed coronal loop model will have several applications and studies to understand the properties of excited MHD waves and plasma dynamics in such tubes. With some modification, the model can be adopted to a coronal loop to reveal its wave and dynamical processes. However, as its first application, we study the vertical kink oscillations evolved into the model loop. These oscillations are excited by a forced periodic driver in the vertical component of velocity, which acts at the top of the photosphere.

This paper is organized as follows. The analytical model of a coronal loop is introduced in Sect. 2. A numerical model

and the results are described in Sect. 3. This paper is concluded by a short summary in Sect. 4.

2. The analytical model of a coronal loop

2.1. MHD equations

We consider a coronal plasma which is described by the ideal magnetohydrodynamic (MHD) equations

$$\frac{\partial \varrho}{\partial t} + \nabla \cdot (\varrho \mathbf{V}) = 0\,, \qquad (1)$$

$$\varrho \frac{\partial \mathbf{V}}{\partial t} + \varrho\,(\mathbf{V}\cdot\nabla)\,\mathbf{V} = -\nabla p + \frac{1}{\mu}(\nabla \times \mathbf{B}) \times \mathbf{B} + \varrho \mathbf{g}\,, \qquad (2)$$

$$\frac{\partial \mathbf{B}}{\partial t} = \nabla \times (\mathbf{V} \times \mathbf{B})\,, \quad \nabla \cdot \mathbf{B} = 0\,, \qquad (3)$$

$$\frac{\partial p}{\partial t} + \mathbf{V}\cdot\nabla p = -\gamma p \nabla \cdot \mathbf{V}\,, \quad p = \frac{k_{\rm B}}{m}\varrho T\,, \qquad (4)$$

where ϱ is mass density, $\mathbf{V}$ represents the plasma velocity, p is a gas pressure, $\mathbf{B}$ is the magnetic field, T is a temperature, $k_{\rm B}$ is Boltzmann's constant, $\gamma = 5/3$ is the adiabatic index, m is a particle mass, that is specified by mean molecular weight of 0.6, and $\mathbf{g} = (0, -g, 0)$ is the gravitational acceleration. The value of g is equal to 274 m s^{-2}.

2.2. Equilibrium conditions

We assume that the above system is invariant along the horizontal coordinate, z ($\partial/\partial z = 0$) and set the z-components of the velocity, $V_{\rm z}$, and magnetic field, $B_{\rm z}$, to zero.

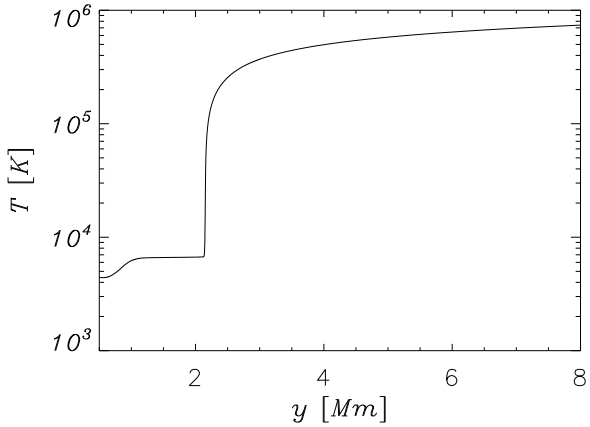

Fig. 1. The profile of hydrostatic solar atmospheric temperature vs. hight y.

In such 2D model, the solar atmosphere is in static equilibrium ($\mathbf{V} = \mathbf{0}$) with the Lorentz force balanced by the pressure gradient and gravity forces, and the divergence-free magnetic field,

$$\frac{1}{\mu}(\nabla \times \mathbf{B}) \times \mathbf{B} - \nabla p + \varrho \mathbf{g} = \mathbf{0}\,, \qquad (5)$$

$$\nabla \cdot \mathbf{B} = 0\,. \qquad (6)$$

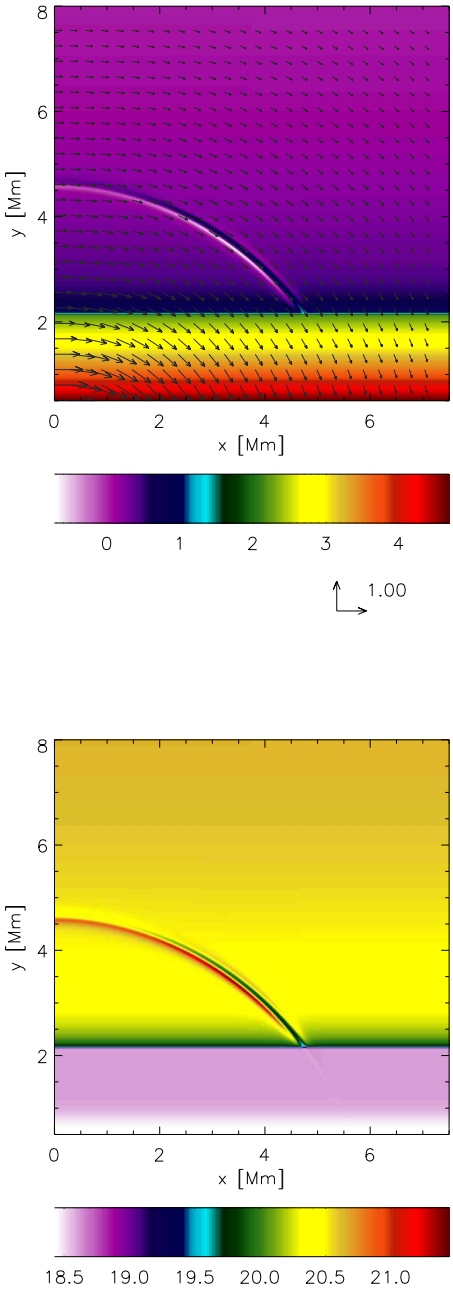

Fig. 2. The top panel: Vectors of equilibrium magnetic field, expressed in units of ≈ 11.4 Gauss, and $\log(\varrho)$ (color maps). The mass density, ϱ, is given in units of 10^{-15} kg m^{-3}. The bottom panel: Logarithm of temperature (expressed in units of 1 MK) profile. The right hand-side of the system (which is symmetric about the vertical $x = 0$ axis) is displayed only.

2.2.1. Hydrostatic atmosphere

A hydrostatic atmosphere corresponds to the magnetic-free ($\mathbf{B} = \mathbf{0}$) case in which the gas pressure gradient is balanced

by the gravity force

$$\nabla p_{\rm h} = \varrho_{\rm h}\mathbf{g}\,. \tag{7}$$

With the use of the ideal gas law given by Eq. (4) and the vertical y-component of Eq. (7), we express the hydrostatic gas pressure and mass density as

$$p_{\rm h}(y) = p_{\rm ref}\,\exp\left(-\int_{y_{\rm r}}^{y}\frac{dy^{'}}{\Lambda(y^{'})}\right)\,,\quad \varrho_{\rm h}(y) = \frac{p_{\rm h}(y)}{g\Lambda(y)}\,, \tag{8}$$

where

$$\Lambda(y) = \frac{k_{\rm B}T(y)}{mg}\,, \tag{9}$$

is the pressure scale-height, and $p_{\rm ref}$ denotes the gas pressure at the reference level $y_{\rm r}$ which we set and hold fixed at $y_{\rm r} = 10$ Mm.

We adopt a realistic plasma temperature profile given by the semi-empirical model of Avrett & Loeser (2008)that is extrapolated into the solar corona (Fig. 1). In this model, the temperature attains a value of about 4300 K at the bottom of the chromosphere ($y \approx 0.6$ Mm), 7×10^3 K at the top of the chromosphere ($y \approx 2.0$ Mm). At the transition region, which is located at $y \simeq 2.1$ Mm, T exhibits an abrupt jump (Fig. 1), and it enhances upto about 0.7×10^6 K in the solar corona at $y = 8$ Mm. Higher in the solar corona, the temperature grows very slowly, tending to its asymptotic value of about 1.6 MK. The temperature profile determines uniquely the equilibrium mass density and gas pressure profiles which fall-off with the height (not shown here).

2.2.2. Magnetic atmosphere

The solenoidal condition of Eq. (6) is automatically satisfied if we express the equilibrium magnetic field with the use of magnetic flux-function ($A(x,y)$) as

$$\mathbf{B} = \nabla\times A\mathbf{e}_{\rm z}, \tag{10}$$

where $\mathbf{e}_{\rm z}$ is a unit vector along z-direction. Setting

$$p = p(x,y) = p(y,A)\,, \tag{11}$$

from Eqs. (5) and (10), we get

$$\varrho(y,A)g = -\frac{\partial p(y,A)}{\partial y}\,. \tag{12}$$

Here we infer the hydrostatic condition along the magnetic field line which is specified by the equation $A = const$. From the x- and y-components of Eq. (5), we obtain the equilibrium equation for a system with translational symmetry (Low 1975; Priest 1982):

$$\nabla^2 A = -\mu\frac{\partial p(y,A)}{\partial A}\,, \tag{13}$$

where $\nabla^2 = \left(\frac{\partial^2}{\partial x^2}+\frac{\partial^2}{\partial y^2}\right)$ is the Laplacian.

We assume now that the flux-function $A(x,y)$ is known. Therefore, from Eqs. (12) and (13), we find the following expressions for ϱ and p (Solov'ev 2010, Kraśkiewicz et al. 2014, Kuźma et al. 2014):

$$\varrho = \varrho_{\rm h} + \frac{1}{\mu g}\left[\frac{\partial}{\partial y}\left(\int\frac{\partial^2 A}{\partial y^2}\frac{\partial A}{\partial x}dx + \frac{1}{2}\left(\frac{\partial A}{\partial x}\right)^2\right) - \frac{\partial A}{\partial y}\nabla^2 A\right]\,, \tag{14}$$

$$p = p_{\rm h} - \frac{1}{2\mu}\left(\frac{\partial A}{\partial x}\right)^2 - \frac{1}{\mu}\int\frac{\partial^2 A}{\partial y^2}\frac{\partial A}{\partial x}dx\,. \tag{15}$$

2.3. A coronal loop

For a coronal loop, we make the following choice:

$$A(x,y) = S_1\log[k^2x^2 + k^2(y+y_{00})^2] + \varepsilon S_1\frac{k^2x^2}{1+k^2[x^2+a(y+y_{00})^2 - x_0^2 - b(y_0+y_{00})^2]}\,, \tag{16}$$

where k is the inverse scale-length, $-y_{00}$ is the vertical coordinate of the singularity in the magnetic field, and a, b, ε, x_0, y_0, and y_{00} are dimensionless parameters. We set them as $a = b = 0.85$, $k = 1$ Mm^{-1}, $x_0 = y_0 = 4$ Mm, $y_{00} = 1$ Mm, $S_1 \approx 11.4$ Gauss Mm, and hold them constant. These loop parameters are chosen to have a small-size loop (averaged radius≈5 Mm), which significantly simplifies numerical simulations. Vectors of magnetic field, resulting from Eq. (16) are illustrated in Fig. 2. As a result of the symmetry, the right-hand side of the system is displayed only, and the magnetic field vectors consist the arcade with a singularity at ($x = 0$, $y = -y_{00}$) Mm.

The first term in the right side of Eq. (16) corresponds to the potential magnetic arcade, in which the magnetic field varies as $1/r$, where r is a radial distance from the axis of symmetry, placed beneath the photosphere, at the location of the singularity. Such potential magnetic field does not alter the hydrostatic state of the solar atmosphere and the equilibrium mass density and a gas pressure remain equal to $\varrho_{\rm h}(y)$ and $p_{\rm h}(y)$, respectively.

Since a purely potential arcade does not lead to any loop structure, we implement the small, non-potential correction (second) term in Eq. (16), which highlights in the body of the magnetic arcade a narrow loop of its radius

$$r_0 = \sqrt{x_0^2 + y_0^2}\,. \tag{17}$$

This correction term is chosen to have the integral in Eq. (15) evaluated analytically. However, the analytical expressions for the equilibrium mass density, $\varrho(x,y)$, and a gas pressure, $p(x,y)$, derived by the symbolic package MAXIMA from Eqs. (14) and (15), are too long to be displayed here.

Within the coronal loop the plasma parameters are significantly different from those in the ambient corona. The correction results in mass density enhancement within the loop. The density (ϱ) within the loop is about twice larger at the loop apex and ten times larger at the loop footpoint than the ambient coronal mass density (Fig. 2). This loop is about four times warmer at its apex and ten times hotter at $x \approx 3$ Mm and $y \approx 3.5$ Mm than the ambient plasma (Fig. 2, bottom). Below the denser strand-like structure which occupies the top layer of the loop, there is the layer of rarefied strand-like plasma at the lower side (Fig. 2, top). The whole strands-like structure is about 500

km wide and the loop is about 15 Mm long with its major radius of about 5 Mm. It should be noted that loop length, width, and major axis etc are the free parameters, and the model can yield the range of loop morphology. We can simply mimic the various kinds of coronal loops with different radius of curvature and height, with different magnetic field strength, and confined plasma with given density and temperature. However, here we only choose the small size of the model loop to avoid computationally extensive numerical calculations. The major aim of this paper is only to introduce our new coronal loop model with a simple example of vertical kink oscillations. Its various applications, and other parametric studies will be taken-up in our future projects.

3. Numerical model for vertical kink oscillations

To solve the 2D, ideal MHD equations numerically, we use the FLASH code (Fryxell et al. 2000; Lee & Deane 2009; Lee 2013), in which a third-order unsplit Godunov-type solver with various slope limiters and Riemann solvers as well as Adaptive Mesh Refinement (AMR) (MacNeice et al. 1999)are implemented. Among a number of options, we choose the minmod slope limiter and the Roe Riemann solver (e.g., Tóth 2000).

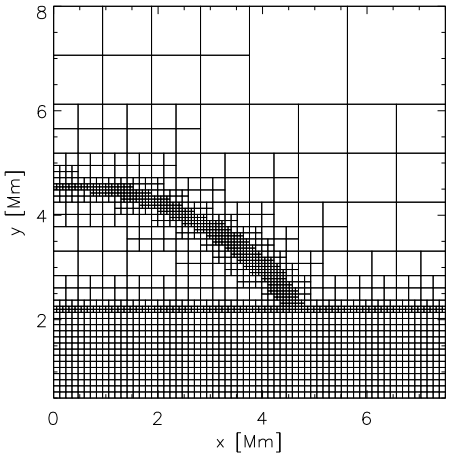

Fig. 3. Blocks system used in the numerical simulations.

We set the simulation box as $(-7.5\,\mathrm{Mm}, 7.5\,\mathrm{Mm}) \times (0.5\,\mathrm{Mm}, 8.0\,\mathrm{Mm})$ and impose time-dependent boundary conditions for all plasma quantities at all four boundaries; at these boundaries we set all plasma quantities to their equilibrium values; the only exception is the bottom boundary, where we additionally place the periodic driver as

$$V_{\mathrm{y}}(x,y,t) = A_{\mathrm{V}}\,\exp\left[-\frac{x^2+(y-y_{\mathrm{d}})^2}{w^2}\right]\sin\left(\frac{2\pi}{P_{\mathrm{d}}}t\right), \quad (18)$$

where A_{V} is the amplitude of the driver, $(0, y_{\mathrm{d}})$ is its spatial position, w denotes its width, and P_{d} is its period. We set $A_{\mathrm{V}} = 3$ km s^{-1}, $y_{\mathrm{d}} = 0.5$ Mm, $w = 1$ Mm, $P_{\mathrm{d}} = 300$ s, and hold them fixed. The driving period $P_{\mathrm{d}} = 300$ s corresponds to the average life-time of a solar granule, as

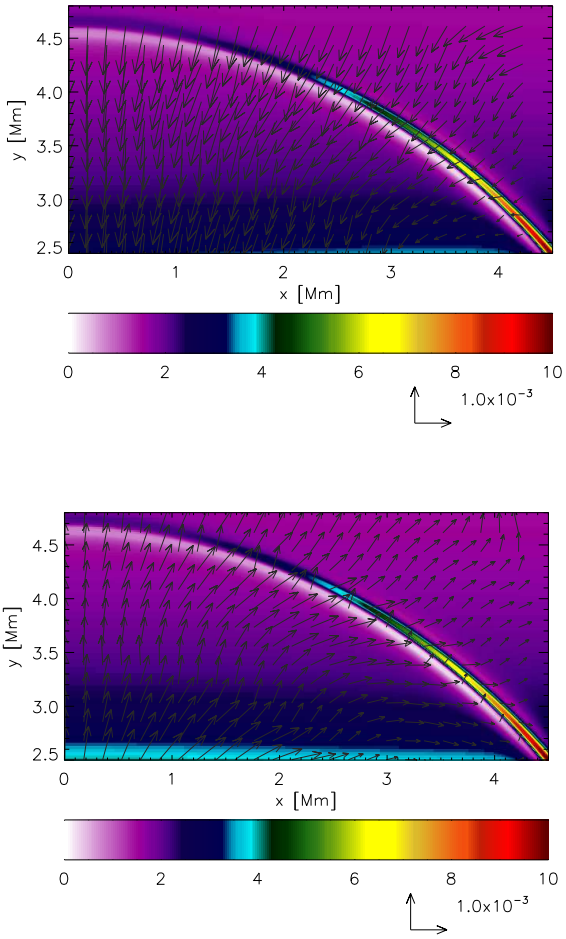

Fig. 4. Temporal evolution of $\varrho(x,y)$ at $t = 550$ s (top) and $t = 700$ s (bottom). Arrows represent plasma velocity. A full-colour version of above figure and movie is available online at www..., Fig4.mpg.

the granules (together with a random coronal flows, which are although not explored in this paper) can be regarded as a real physical driver of decay-less coronal loop oscillations (Valery Nakariakov, private communication).

In our present work, we use an AMR grid with a minimum (maximum) level of refinement set to 3 (8). We performed the grid convergence studies by refining the grid by a factor of two. As the numerical results remained essentially same for the grid of maximum block levels 7 and 8, we adopted the latter to get the results presented in this paper.

Note that small-size blocks of numerical grid occupy the altitude upto $y \approx 5$ Mm, below the solar transition region and in the neighborhood of the loop (Fig. 3), and every numerical block consists of 8×8 identical numerical cells. This results in an excellent resolution of steep spatial profiles, and greatly reduces the numerical diffusion in these regions.

Figure 4 shows the spatial profiles of $\varrho(x,y)$ at two timespans. Note that the right-hand part of the simulation region is displayed only. As a result of the driver, essentially fast magnetoacoustic-gravity waves are excited in the system. The fast magnetoacoustic waves are quasi-isotropic

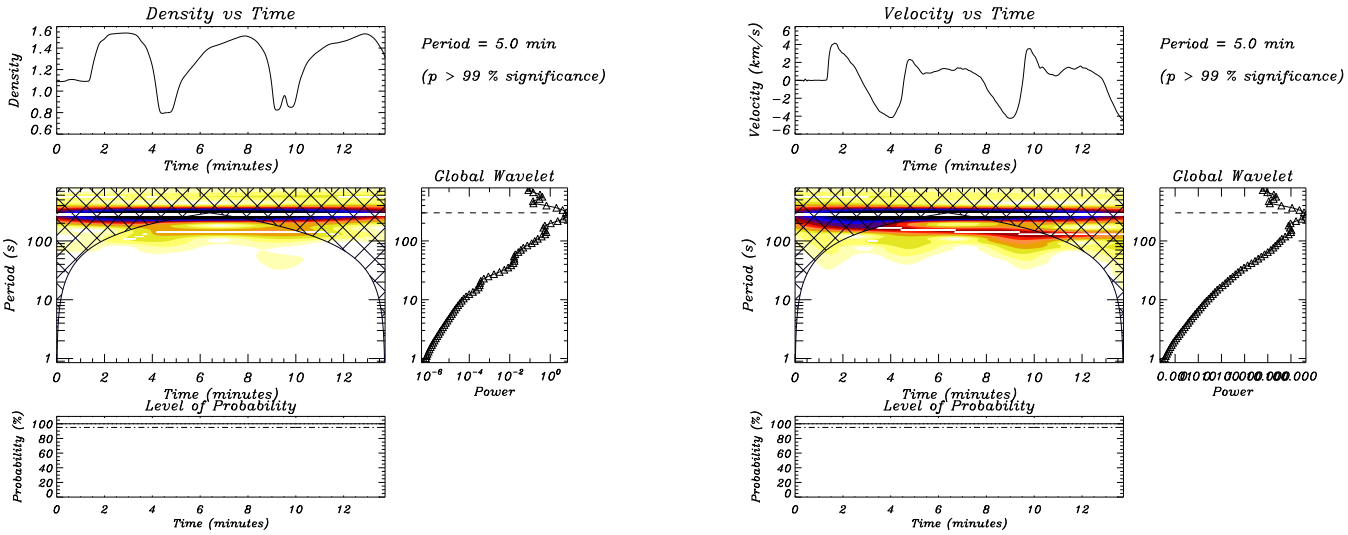

Fig. 5. Time-signatures of ϱ (top-left) and $V_{\rm y}$ (top-right) collected at $(x = 0, y = 4.5)$ Mm, and their wavelet spectra.

and they propagate upwards across the curved magnetic field lines. At $t = 550$ s (top) and $t = 700$ s (bottom), the plasma is moving downwards (upwards) and the apex of the loop attains approximately its lowest (highest) position of ≈ 4.6 Mm (≈ 4.7 Mm), oscillating with the amplitude of about 100 km. It should be noted that the vertical kink oscillations of a curved coronal loop are fundamentally different from horizontal kink modes, since they are confined to the loop plane and can lead to the change of its length. These oscillations are well seen in Fig. 5 which illustrates the time-signature of ϱ (top-left) and $V_{\rm y}$ (top-right) collected at the point ($x = 0$, $y = 4.5$) Mm, settled just below the apex. From this figure we clearly see that the quasi-periodic oscillations are present in the system, and the wave-period of these oscillations is equal to the driving period, $P_{\rm d} = 300$ s. Indeed, Figure 5 (bottom) illustrates wavelet spectra of these time-signatures, from which we infer that the velocity time-signature is a combination of 5 min and 3 min waveperiods, but the 5 min waveperiod is predominant. The periodogram analyses (Scargle 1982) also show the presence of significant ($> 3\sigma$) power peaks around 5 min waveperiod in both mass density as well as velocity time-profiles, which are consistent with the wavelet power spectral analyses. The amplitude of these oscillations in $V_{\rm y}$ is about 1.1 km s^{-1} (Fig. 5, top-right). It should be noted that the phase-difference between velocity and density variations with time is $\pi/4$ (quarter period), which is a typical property of the fundamental kink oscillations excited in a loop.

4. Summary

In the present paper, we have presented for the first time the analytical and numerical models of a solar coronal loop, which is embedded in a gravitationally stratified solar corona. These models are based on the analytical models of Solov'ev (2010).The Kraśkiewicz et al. (2014) and Kuźma et al. (2014)report can also be referred for the detailed mathematical formulation of the analytical and numerical models. Using these models, we performed the 2D numerical simulations of the vertical kink oscillations of this loop excited by the forced periodic driver that acts at the top of the photosphere, centrally below the apex of the loop.

The numerical simulations adapt the realistic model of the hydrostatic solar atmosphere in the FLASH code and a slightly modified potential magnetic field. Our model exhibits the formation of the quasi-periodic vertical oscillations of their wave-period equal to the driving wave-period of 300 s and their velocity amplitude is about 1.2 km s^{-1}, while the loop apex oscillates with its amplitude of 100 km. These values match the recent observational findings of Nisticó et al. (2013) and Anfinogentov et al. (2013).

We note here that the implemented driver mimics a downdraft associated with a solar granule as the driving period is set to the life-time of a granule, that is 300 s, and its amplitude is 3 km s^{-1}. However, the latter value seems to be larger by a factor of about 3 than the downdraft speed. We have verified by numerical experiments that a lower amplitude of the driver resulted in less pronounced oscillations (not shown). Moreover, to simplify numerical simulations we have chosen the coronal loop of only about 15 Mm long, which is at least an order of magnitude too short than a typical coronal loop. In the latter case, the fast magnetoacoustic waves would experience more spatial spreading while propagating from the launching place upwards towards the typical loop apex and covering a long distance. As a result of that this apex would be affected by less energetic signal and it would experience lower amplitude oscillations. In this case a larger amplitude of the periodic driver would be required or a driver can be set higher-up, somewhere in the solar corona, modelling its random velocity field. Qualitatively, we can state that the oscillation amplitude should decline with the loop length (L) and it should grow with the amplitude of the forced driver (A_v). Such parametric studies would be important for impulsively excited waves with the non-forced drivers, which will be devoted to our future study using the newly developed coronal loop model.

Acknowledgements. We thank the referee for his/her valuable comments which improved the manuscript considerably. AKS thanks Prof. K. Murawski and UMCS, Lublin for providing a visit fund during September-October 2014 during which He contributed to the project. The work has also been supported by a Marie Curie International Research Staff Exchange Scheme Fellowship within the 7th European

Community Framework Program. The software used in this work was in part developed by the DOE-supported ASCI/Alliance Center for Astrophysical Thermonuclear Flashes at the University of Chicago. The visualizations of the simulation variables have been carried out using the IDL (Interactive Data Language) software package.

References

[1] Anfinogentov, S., Nisticò, G., & Nakariakov, V. M. 2013, A&A, 560, AA107
[2] Antolin, P., Yokoyama, T., & Van Doorsselaere, T. 2014, ApJ, 787, LL22
[3] Aschwanden, M. J., Fletcher, L., Schrijver, C. J., & Alexander, D. 1999, ApJ, 520, 880
[4] Aschwanden, M. J., Nightingale, R. W., & Alexander, D. 2000, ApJ, 541, 1059
[5] Aschwanden, M. J., & Schrijver, C. J. 2011, ApJ, 736, 102
[6] Avrett, E. H., & Loeser, R. 2008, ApJS, 175, 229
[7] De Moortel, I., & Nakariakov, V. M. 2012, Royal Society of London Philosophical Transactions Series A, 370, 3193
[8] Fryxell, B., Olson, K., Ricker, P., et al. 2000, ApJS, 131, 273
[9] Gruszecki, M., Murawski, K., Selwa, M., & Ofman, L. 2006, A&A, 460, 887
[10] Kráskiewicz, J., Murawski, K., Solov'ev, A. & Srivastava, A.K. 2014, Sol. Phys., submitted.
[11] Kuźma, B., Murawski, K., Solov'ev, A. 2014, A&A, submitted.
[12] Lee, D. 2013, Journal of Computational Physics, 243, 269
[13] Lee, D. & Deane, A. E. 2009, Journal of Computational Physics, 228, 952
[14] Low, B. C. 1975, ApJ, 197, 251
[15] Luna, M., Terradas, J., Oliver, R., & Ballester, J. L. 2010, ApJ, 716, 1371
[16] MacNeice, P., Spicer, D. S., & Antiochos, S. 1999, 8th SOHO Workshop: Plasma Dynamics and Diagnostics in the Solar Transition Region and Corona, 446, 457
[17] Nisticò, G., Nakariakov, V. M., & Verwichte, E. 2013, A&A, 552, AA57
[18] Ofman, L. 2009, ApJ, 694, 502
[19] Ofman, L., & Wang, T. J. 2008, A&A, 482, L9
[20] Pascoe, D. J. 2014, Research in Astronomy and Astrophysics, 14, 805
[21] Priest, E. R. 1982, Dordrecht, Holland ; Boston : D. Reidel Pub. Co. ; Hingham,,
[22] Scargle, J. D. 1982, ApJ, 263, 835
[23] Selwa, M., Solanki, S. K., & Ofman, L. 2011, ApJ, 728, 87
[24] Solov'ev, A. A. 2010, Astronomy Reports, 54, 86
[25] Srivastava, A. K., & Goossens, M. 2013, ApJ, 777, 17
[26] Tóth, G. 2000, Journal of Computational Physics, 161, 605
[27] Verwichte, E., Aschwanden, M. J., Van Doorsselaere, T., Foullon, C., & Nakariakov, V. M. 2009, ApJ, 698, 397
[28] Wang, T. J., & Solanki, S. K. 2004, A&A, 421, L33
[29] Wang, T. J., Solanki, S. K., & Selwa, M. 2008, A&A, 489, 1307
[30] White, R. S., Verwichte, E., & Foullon, C. 2012, A&A, 545, AA129